PERFORMANCE COMPARISON OF THE BLENDED WING BODY AND TUBE-AND-WING CONFIGURATIONS

Jai Ahuja, Christian Perron, Reina D. Bermudez Rivera, Jimmy C. Tai & Dimitri N. Mavris

Aerospace Systems Design Laboratory, Daniel Guggenheim School of Aerospace Engineering, Georgia Institute of Technology, Atlanta, GA, 30332, USA

Abstract

This paper focuses on quantifying the impacts of the airframe configuration change on the performance differences between a tube-and-wing and a blended wing body aircraft. Both aircraft are sized for the same mission requirements: a 5,000 nmi design range carrying 225 passengers. Also, both aircraft initially use the same engine, designed for a 2030 time frame, with an uninstalled 43,000 lb sea-level-static thrust. A parametric geometry is created for both concepts based on relevant public information. The tube-and-wing notional geometry is derived from the existing Boeing 767-300ER, whereas JetZero's proposed concept inspires the blended wing body geometry. These geometries are then optimized using computational fluid dynamics and gradient-free approaches. Drag polars for each optimized model, spanning the expected operating envelope, are generated using computational fluid dynamics simulations and multi-fidelity surrogate models. Mission analysis is then performed using these drag polars for the blended wing body, a conventional tube-and-wing variant with metallic structures, and an advanced tube-and-wing version that uses composites for the structural material. The results show that the blended wing body operates with a 15-20% higher lift-over-drag during cruise, a 24% lower fuel burn for the design mission, and a 15% reduction in ramp weight relative to the conventional tube-and-wing. These differences drop to 20% for the design mission fuel burn and 10% for the ramp weight relative to the advanced tube-and-wing. In a second comparison where the engines are re-sized and optimized separately for each configuration, the blended wing body demonstrates a 25% improvement in block fuel and a 16% reduction in ramp weight relative to the conventional tube-and-wing, which decreases to 21% and 10% relative to the advanced tube-and-wing.

Keywords: blended wing body, tube-and-wing, aerodynamic shape optimization, multi-fidelity, system analysis

1 Introduction

The aviation sector avidly seeks novel approaches for increasing fuel efficiency to lower operational costs and meet emissions reduction targets. The International Air Transport Association (IATA) has set a target to halve net aviation carbon dioxide emissions by 2050 relative to 2005 levels [1]. Of the numerous ideas put forward by industry and academia for sustainable aviation, the blended wing body (BWB) concept targets the fundamental performance deficiencies of the ubiquitous tube-and-wing (TNW) configuration. The TNW primarily produces lift through its wings, with the fuselage being a rather inefficient lifting body with a meager lift-over-drag ratio. In contrast, the entire BWB airframe is a lifting surface, making it more aerodynamically efficient than the TNW. Furthermore, the BWB's gradual blend of wing and body, lack of an empennage, and smaller wetted area decrease drag relative to a TNW of similar passenger capacity. An additional benefit of the BWB is the ability to mount engines above the airframe, which has the potential to increase aerodynamic efficiency,

reduce noise emissions by shielding engine noise [2, 3, 4], and allow for higher bypass ratio engines with increased propulsive efficiency [5].

One of the early comprehensive studies on the BWB was conducted in the late 1990s as a collaboration among Boeing, NASA, and university partners [6]. It focused on a BWB featuring boundary layer ingesting engines with a passenger capacity of 800, a range of 7,000 nmi, and a cruise speed of Mach 0.85. The study showed a 15% reduction in takeoff weight, a 27% reduction in fuel burn, and a 20% higher lift-over-drag compared to a conventional TNW sized for the same payload and range. Boeing conducted a follow-up study in the early 2000s [7], where the Boeing BWB-450 was designed for a reduced payload of 468 passengers with a 7,750 nmi range, more in line with market forecast data. This concept used pylon-mounted engines to reduce the technological risk. Compared to the Airbus A380-700 for the same payload and range, the BWB-450 showed an 18% reduction in takeoff weight and a 32% reduction in fuel burn per seat. These promising results would encourage future studies into the BWB as the next evolution in commercial passenger aircraft.

The Silent Aircraft Initiative studies by Cambridge University-MIT in the mid-2000s focused on designing a BWB concept to reduce noise and carried a design payload of 215 passengers. Featuring embedded boundary layer ingesting engines, the resulting design had a roughly 25% improvement in passenger miles flown per gallon of fuel compared to existing commercial aircraft [8], although the reference aircraft were not identical in terms of payload and range. This aircraft would then become the starting point of the work conducted by Boeing and NASA in the late 2000s to design realistic BWB aircraft that significantly reduced noise and fuel burn with technologies projected to be available in 2020; these would become the HWB N2A and N2B [9]. The N2A had podded engines whereas the N2B retained the characteristic of boundary layer ingesting engines from its predecessor. Both aircraft had a maximum payload of 103,000 lb, a range of 6000 nmi, and a cruise speed around Mach 0.8 [9]. The N2A achieved a 29% reduction in fuel burn and the N2B achieved a 25% reduction in fuel burn compared to the A330-200FX conventional TNW freighter [9].

In more recent work, researchers from Delft University of Technology compared optimized BWB and TNW designs for the same design requirements [10]. They designed three BWB baselines for 150, 250, and 400 passengers, then optimized them using an in-house program. The TNWs were designed based on specifications from the A320-300, B767-300ER, and B777-300 and then optimized with the same program. They compared the aerodynamic performance of the BWB and TNW aircraft using low-fidelity semi-empirical methods for drag prediction coupled to a vortex lattice solver. Their results showed the BWB having a 12–23% higher aerodynamic efficiency for the 250 and 400-passenger categories. No mission analysis was conducted to estimate fuel burn. Around the same time, DZYNE Technologies Inc. published papers regarding their design of the Ascent 1000, a 112–120 passenger BWB for regional jet markets with a design range of 3,200 nmi [11, 12]. The Ascent 1000 claims an over 60% fuel burn reduction and an 80% emissions reduction compared to the 2005 best-in-class ERJ-190 regional jet [11].

The current state-of-the-art BWB, encapsulating the past three decades of BWB design experience and knowledge, is the concept proposed by JetZero[1]. Their planned entry into service is in the 2030s, with a full-scale demonstrator scheduled to take flight in 2027. The aircraft is intended to fill the same niche as the Boeing 767 and is claimed to reduce fuel burn by about 50%[2].

All previous work demonstrates that the BWB is likely to outperform the TNW and is a rather promising solution for a greener future. However, a few deficiencies in past work warrant a fresh look at the performance comparison between the BWB and the TNW. For starters, the early work by Boeing-NASA on the BWB looked at passenger capacities that are no longer as relevant in today's market. Although later work looked at smaller passenger capacities, many failed to provide an "apples-to-apples" comparison between the BWB and the TNW by enforcing the same payload-range requirements, optimizing both airframes, and considering similar levels of technology on the airframe/propulsion system.

[1] "Why JetZero", JetZero, last accessed July 9, 2024. https://www.jetzero.aero/why-jetzero.

[2] Jacopo Prisco, "JetZero: Groundbreaking 'blended-wing' demonstrator plane cleared to fly", CNN, last accessed July 9, 2024. https://www.cnn.com/travel/jetzero-pathfinder-subscale-demonstrator/index.html.

Also, the impacts of the configuration change, i.e., the difference in performance solely due to the airframe change, for the same engine, were not quantified in these past studies. Detailed mission analysis and high-fidelity aerodynamics modeling were also missing in some previous efforts. Many early BWB studies also included boundary layer ingesting engines which favored performance, but this technology is unlikely to mature sufficiently to be featured on aircraft by 2030. This study addresses the aforementioned shortcomings and provides the latest perspective on quantifying the benefit of the BWB configuration over the TNW. Specifically, this study look at payloads, ranges, and technologies in line with industry's vision for 2030. The following section outlines the work plan.

2 Problem Formulation

The primary objective behind this study is to quantify the performance benefit of the BWB configuration over a conventional TNW. Specifically, we compare the aerodynamic efficiency of an optimized BWB airframe to an optimized TNW airframe at the same Mach number and altitude that best represents cruise conditions for both. We also perform mission analysis and compare system-level metrics like block fuel and ramp weight between the two aircraft configurations.

We establish a common design and analysis procedure for both to accomplish these tasks and provide a fair comparison between the two vehicles. We start by designing a baseline geometry for both airframes, discussed in Secs. 3.1 and 3.2. The airframes are sized to accommodate 225 passengers, in a three-class layout, and carry enough fuel for a 5,000 nmi design mission followed by a 200 nmi reserve mission. The nacelles and pylons are not included in either geometry, but their drag contributions and interference effects are estimated separately and included in the mission analysis. Then, both geometries are optimized using computational fluid dynamics (CFD), as discussed in Sec. 3.4, to give each configuration the best possible chance of achieving good aerodynamic performance. Following this step, we generate aerodynamic data to form mission drag polars for each optimized geometry, as discussed in Sec. 3.5. These mission polars are a set of drag polars spanning the expected operating envelope of both vehicles.

For mission analysis, we also define an engine model for each vehicle. To isolate the impacts of the TNW to BWB airframe change on the performance metrics, the same engine must be used on both vehicle models. This implies an engine that is identical in all respects, i.e., in mechanical and thermodynamic characteristics. Any differences in cycle, engine lapse rate, component design and weight, and thrust class will influence the performance disparity between the two vehicles, thus making it harder to isolate the airframe's contributions. As such, we develop a common engine model suitable to power both configurations throughout their design mission without severely compromising the performance of either concept. This engine design process is discussed in Sec. 3.6. We also acknowledge the criticism that a common engine for both the TNW and BWB is unlikely to be optimal for either. To get the best possible performance for each configuration, the engine should be resized and the cycle should be re-designed to best match the airframe. As such, we also include another comparison point between the two vehicles where the engine is specifically optimized for each configuration. The engine design process for this comparison is also presented in Sec. 3.6.

Once the engine and aerodynamics models are complete, we conduct mission analysis for both the BWB and TNW, as presented in Sec. 3.7. We model two variants of the TNW in our mission analysis with different structural materials to represent different technology levels. We thoughtfully ensure that the mission assumptions and modeling fidelity are the same to avoid any biases in the comparison. In addition to comparing block fuel and gross weight for the design mission, we also consider a shorter economic mission of 900 nmi. Weight breakdowns of the aircraft are also compared. Sec. 4 presents and discusses these results in detail.

3 Methodology

The following section goes over the development of both baseline airframes. We also present details on the aerodynamic modeling, optimization strategy, and drag polar generation. We discuss

the engine design that will be used for both configurations. Finally, we outline the system analysis procedure which will provide the key results of our comparison.

3.1 Blended Wing Body Baseline Development

As outlined previously, the BWB concept has been studied for decades, but a full-scale prototype has yet to be manufactured and flown. Therefore, the current BWB baseline is derived from recent concepts in the literature. Our design takes inspiration from JetZero's aircraft concept as it represents the latest development of BWB technology and is arguably the closest to a physical demonstrator. Figure 1 presents our BWB baseline geometry as well as some key geometric information. This geometry is parametric and was created using Engineering Sketch Pad (ESP), an open-source geometry modeling tool [13]. The internal volume of the vehicle is sufficient to carry 225 passengers in a three-class layout with luggage stored in LD-2 containers carried within the shoulders of the aircraft, i.e., the transition regions between the center body and the wing, as shown in Fig. 2. The overall planform outline is loosely based on images, press releases, and news articles,[3,4] that were available in the public domain at the time of writing. The shape of the centerbody is created with an intricate set of splines whereas the wing airfoil stack is parameterized with the class/shape transformation (CST) method [14]. We use the SAX-40 [8] published airfoils and twist distribution to establish the baseline wing and winglet shapes. The wing twist was then further adjusted manually to improve the performance of the baseline and provide a better starting point for the aerodynamic optimization.

Overall Planform Area (excl. winglets)	5738 sqft
Overall Aspect Ratio (excl. winglets)	5.36
Centrebody LE Sweep	62 deg
Outboard Wing Taper Ratio	0.495
Outboard Wing LE Sweep	34 deg
Outboard Wing Dihedral	4 deg

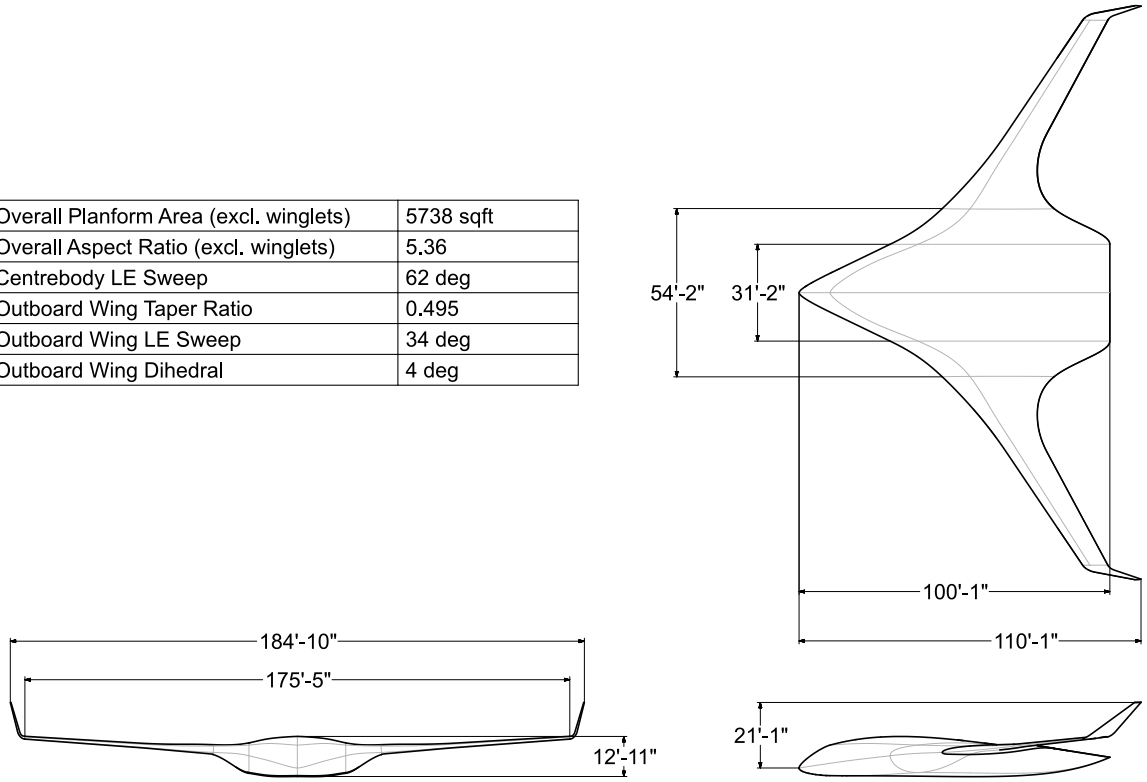

Figure 1 – Baseline blended wing body aircraft inspired by recent aircraft concepts

[3]Guy Norris and Graham Warwick, "JetZero Unveils Midmarket Airliner And Air Force Tanker BWB Plan", Aviation Week, April 21, 2023, last accessed July 11, 2024, https://aviationweek.com/aerospace/emerging-technologies/jetzero-unveils-midmarket-airliner-air-force-tanker-bwb-plan.

[4]Adam Gavine, "A first look inside JetZero's blended wing body", Aircraft Interior International, May 17, 2023, last accessed July 11, 2024, https://www.aircraftinteriorsinternational.com/news/cabin-design/a-first-look-inside-jetzeros-blended-wing-body.html

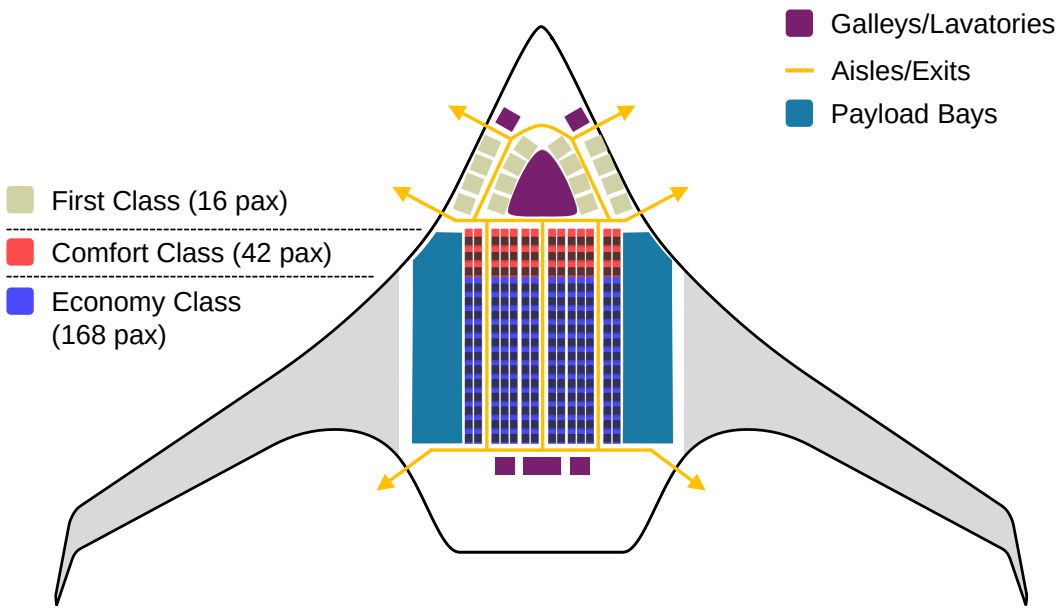

Figure 2 – Notional internal layout for the current BWB baseline aircraft

3.2 Tube and Wing Baseline Development

The TNW baseline geometry is notionally inspired by a Boeing 767-300ER. This aircraft, using the "76Z" three-class seat layout from Delta Air Lines,[5] can accommodate 225 passengers. The TNW geometry is created in ESP using dimensions derived from the three-views in the Boeing 767 series airport planning manual [15]. Figure 3 shows the three-views of our geometry along with some key design characteristics. The Boeing 767-300ER wing was originally designed without winglets, however, some models have since been retrofitted to include them. We chose to include winglets since most modern TNW aircraft have them for enhanced aerodynamic performance. Excluding the winglets would unfairly penalize the TNW relative to the BWB, which also features such components. We initially derived the TNW baseline wing geometry airfoil stack from the NASA Common Research Model (CRM) [16], but then modified the twist distribution to get a better performing starting point. The vertical tail uses a NACA 64A011 airfoil, like the ONERA CRM vertical tail [17], whereas the horizontal tail airfoil is based on a CRM horizontal tail section extracted near the root.

3.3 CFD Modeling

To minimize the computational expense of this study without significantly impacting accuracy, we use a combination of inviscid and viscous CFD simulations for optimization and drag polar generation. We use Siemens STAR-CCM+ for both the Euler and Reynolds-Averaged Navier Stokes (RANS) CFD simulations, assuming steady-state conditions. We select an implicit time integration scheme with a third-order Monotonic Upstream-centered Scheme for Conservation Laws (MUSCL) central difference spatial discretization, with the advection upstream splitting method, flux vector splitting (AUSM+ FVS) [18] and the Venkatakrishnan limiter [19] for evaluating the inviscid fluxes. For the RANS cases, we assume standard atmosphere conditions, fully turbulent flow, and choose the k-ω shear stress transport (SST) turbulence model [20]. We define the stopping conditions for both the Euler and RANS cases as follows: the change in drag coefficient (C_D) is less than one drag count and the change in lift coefficient (C_L) is less than 0.001 over 1000 iterations. Both conditions need to be satisfied for termination. We set up a hemispherical domain for the farfield with a radius that is roughly 50 times the half-span of each configuration. We use the overall planform area and the wing planform area, shown in Figs. 1 and 3, as the reference area for the aerodynamic coefficients of the BWB and TNW respectively.

[5] "Boeing 767-300ER Seat Specifications", Delta Air Lines, last accessed July 11, 2024, https://www.delta.com/us/en/aircraft/boeing/767-300er.

Wing Planform Area (excl. winglets)	3277 sqft
Wing Aspect Ratio (excl. winglets)	7.43
Inboard Wing Taper Ratio	0.635
Outboard Wing Taper Ratio	0.301
Inboard Wing Sweep	28.74 deg
Outboard Wing Sweep	31.38 deg
Inboard Wing Dihedral	5.5 deg
Outboard Wing Dihedral	5.2 deg
HT Planform Area	834 sqft
HT Aspect Ratio	4.48
HT Taper Ratio	0.264
HT Sweep	32.68 deg
HT Dihedral	9.0 deg
VT Planform Area	325 sqft
VT Aspect Ratio	1.58
VT Taper Ratio	0.372
VT Sweep	39.5 deg

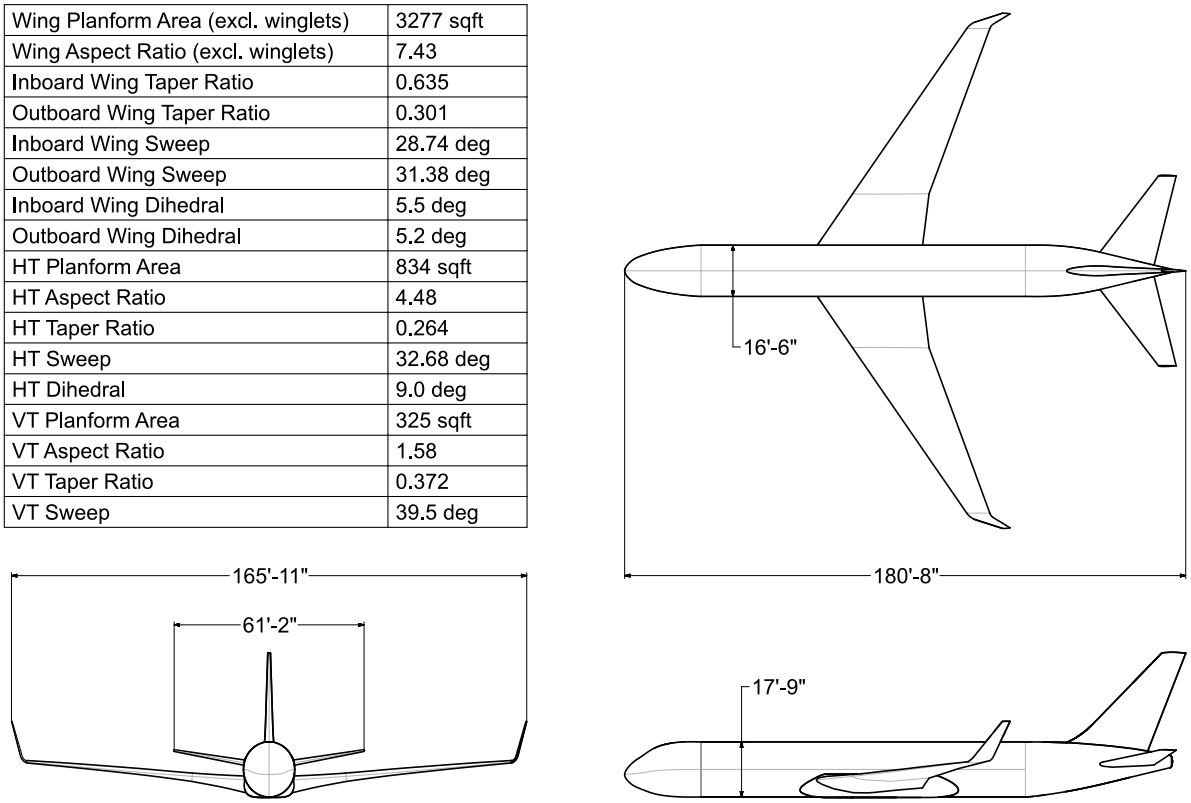

Figure 3 – Baseline tube and wing aircraft notionally inspired by the Boeing 767-300ER with winglets

We use an unstructured polyhedral grid which includes prism layers for the RANS cases to capture the boundary layer gradients over the surfaces. Through simple turbulent flat plate relations, we estimated the total boundary layer thickness, near wall spacing, and the number of prism layers required to maintain a wall $y^+ < 1$ over most of the airframe surface. We conducted a RANS grid sensitivity study for both configurations, run at Mach 0.8, 40,000 ft altitude, and a fixed angle of attack of 3 degrees. Figure 4 presents the mesh sensitivity results for the BWB cases whereas Fig. 5 shows the TNW results. For both the BWB and the TNW, we chose the grid settings that yield a mesh size of about 50M cells in an effort to balance cost and accuracy. The difference in lift-over-drag (L/D) for the selected grid compared to the finest mesh is about 1% for the TNW and approximately 0.5% for the BWB and was thus deemed acceptable.

3.4 Optimization Strategy

While the baseline BWB and TNW aircraft described in Secs. 3.1 and 3.2 provide a reasonable outline of their respective airframe, some details were defined arbitrarily and could easily skew the results. To fairly compare both configurations, we must then perfect these details and optimize the airframe to give each concept the best potential for success. Specifically, we focus on the camber and twist of the main lifting surfaces which can substantially impact the aircraft's aerodynamic efficiency. The planform shapes were fixed in the optimization process. We note that since many aspects of this study are conceptual, the goal of this optimization is not to be final, but rather to provide credible performance estimates for the subsequent mission analysis.

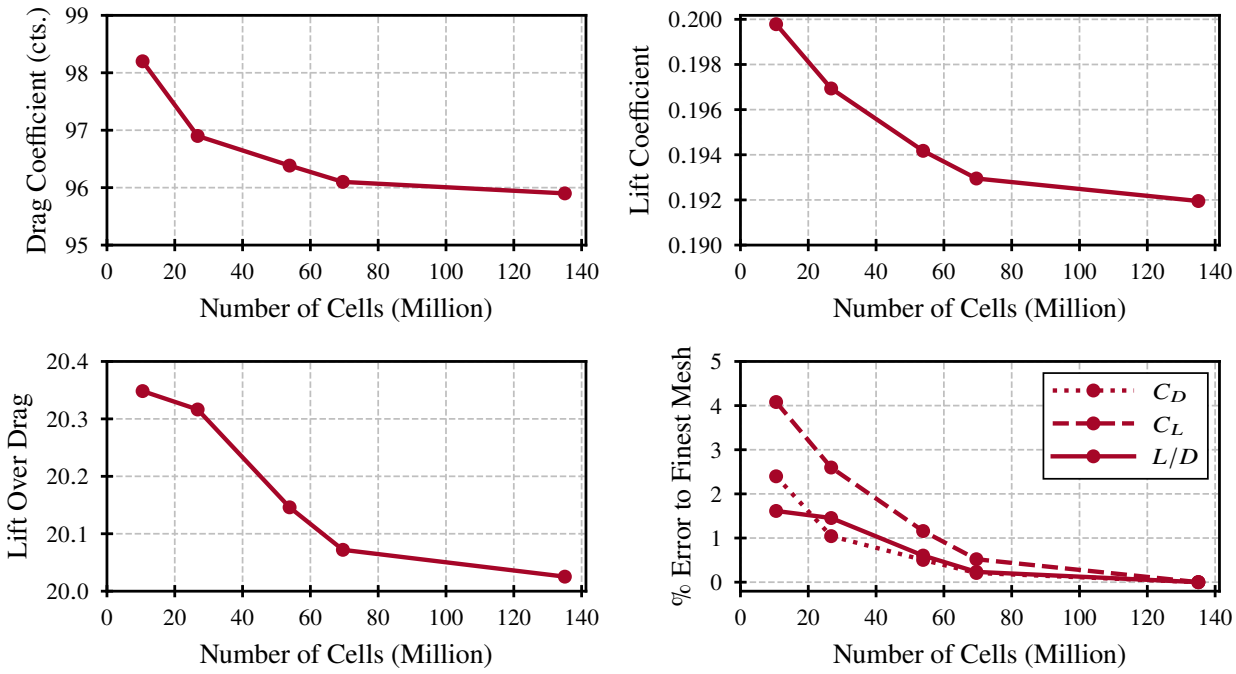

Figure 4 – BWB RANS grid refinement study results

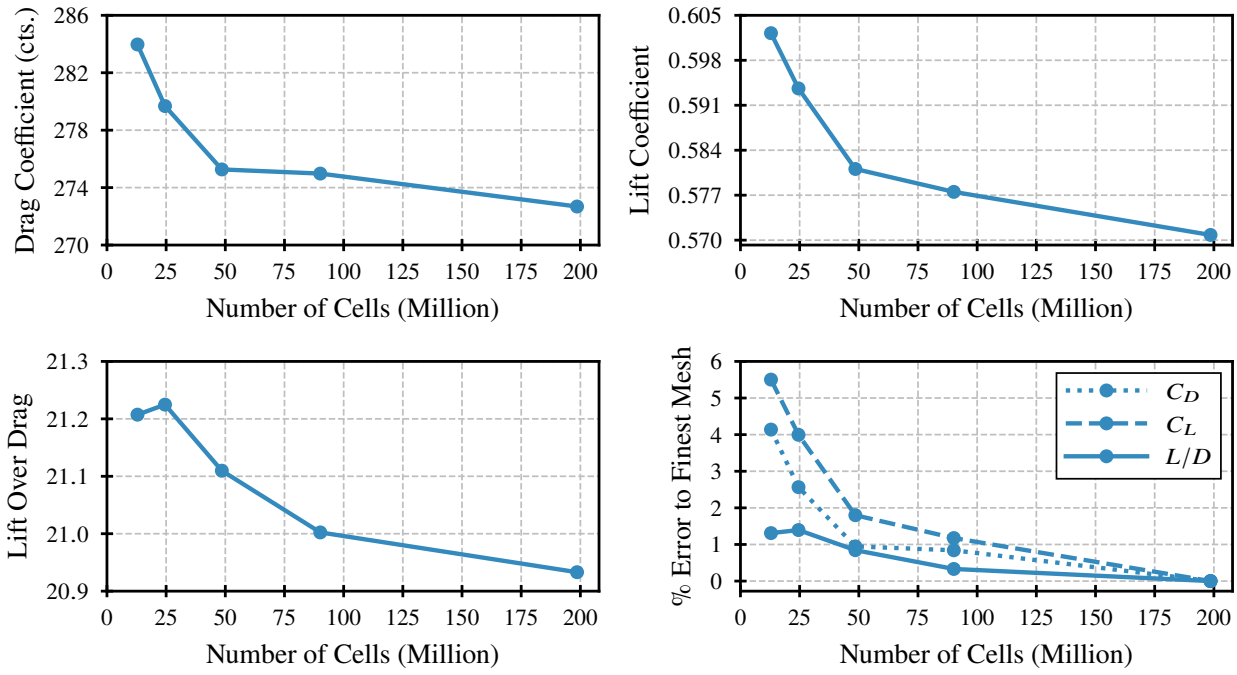

Figure 5 – TNW RANS grid refinement study results

3.4.1 Problem Formulation

The objective of the current optimization is to maximize the vehicle lift-over-drag ratio at the design cruise conditions (Mach number of 0.8 and altitude of 40,000 ft). The outboard wing of the BWB baseline is defined by six span-wise stations with an additional two stations for the winglets. Similarly, the wing of the TNW is defined with seven span-wise stations with two more for the winglets. At each station, the airfoil shape is controlled by eight CST coefficients for both the upper and lower surfaces, for a total of 16 coefficients per station. We opted to only modify the camber line of the baseline airfoils

and to leave their thickness distribution untouched since the latter has strong consequences on the wing structural weight, which we calculate using only low-fidelity semi-empirical relations. In doing so, the degrees of freedom of the airfoil shape are cut in half (see Ref. [14] for a relation between CST coefficients and camber) and only eight design variables are needed per station. Additionally, each wing and winglet station is given a twist angle, and the vehicle angle-of-attack is controlled independently. The above camber, twist, and angle-of-attack, parameters amount to 73 and 82 design variables for the BWB and TNW aircraft respectively. Each design space is centered around their baseline geometry and angle-of-attack for max L/D, with specified bounds of ± 0.075 for the camber CST coefficients, ± 2 degrees for the station twist, and ± 2 degrees for the angle-of-attack.

3.4.2 Bayesian Adaptive Sampling

The optimization process is performed using a Bayesian adaptive sampling method. We used a similar process in Ref. [21] for an aeropropulsive optimization problem and it has been an effective, and robust approach for the optimization of expensive analyses such as CFD. Previous sources describe this method in depth [22, 23], and so we will only provide a summary. The optimization starts with training a Kriging surrogate model using a set of initial samples. These first samples are uniformly selected from the design space and form what we refer to as the “warm start”. In this study, a sample size of 100 designs is considered. The Kriging model allows one to predict the performance of a new unsampled design with some measure of uncertainty. This information is combined into an infill criterion, and specifically, we use the expected improvement (EI) criterion described by Jones et al. [22]. By minimizing this criterion in a sub-optimization problem, we determine what design to evaluate next to progress toward the optimum while exploring the unsampled regions of the design space. Normally, a new Kriging model is trained every time a new design is evaluated, and the process is repeated until convergence. However, we select the next five candidate designs, which we evaluate concurrently. This selection is done using the “Kriging believer” process as explained by Ginsbourger et al. [24]. By choosing multiple designs at once, we can better utilize available computing resources and find the optimum faster. The optimization is stopped once the EI value reaches a small threshold, indicating that the chances of finding a better design are low.

3.4.3 Active Subspace Method

Generally, the Bayesian adaptive sampling method tends to struggle with problems having many design variables such as in this study. This is mostly related to high-dimensional phenomena described as the "curse of dimensionality" [25] and the "concentration of distances" [26]. To overcome these issues, we employ the active subspace method [27] to compress the design space into a lower-dimensional one. The goal of this method is to identify a linear subspace within the design space that best explains the relation between an output of interest and a high-dimensional input. The outcome is a set of variables, called active variables, that represents a linear combination of all the original design variables. With this transformation, the optimization can proceed using a few active variables instead of the many original variables. In this study, the 73 and 82 design variables of the BWB and TNW respectively, are reduced to only six active variables each. Unlike the original active subspace method from Constantine et al. [27] which requires the gradient information, we use a gradient-free variant described in Refs. [28, 29] for this study. This avoids the challenge and the computational cost of computing the gradient of the objective function, which we also do not require for the optimization. To further reduce the computational effort, the active subspace is extracted using lower-fidelity results from an inviscid simulation. Previously Ref. [30] demonstrated that this multi-fidelity approach provided a good approximation of the actual active subspace, yet at a substantially lower cost. We also note that we previously used a similar approach in Ref. [21] for a different aeropropulsive problem.

3.5 Mission Drag Polar Generation

Given the cruise point optimized BWB and TNW geometries, we need estimates for their aerodynamic performance over the entire expected operating envelope. Specifically, the mission analysis requires

a drag polar for different Mach and altitude combinations for each configuration. Although low-fidelity semi-empirical methods, such as those described in Ref. [31], are appropriate for conventional tube-and-wing aircraft sizing and mission analysis, they are less so for more unconventional configurations such as the BWB. Compared to the TNW, the BWB historical, experimental, and computational data are scarce, which must be compensated by higher-order physics modeling. However, differences in aerodynamics model fidelity would be a source of bias when comparing the TNW and BWB. Thus, both vehicles need the same level of fidelity for the mission drag polars. This exercise, if conducted entirely using fine grid RANS CFD simulations, would be quite costly and time-consuming. As such, we leverage multi-fidelity techniques to lower the computational cost without significantly compromising accuracy.

The main idea is that lower fidelity analyses, such as Euler CFD, capture most of the physics of interest and thus the general shape of the polar fairly accurately. Euler CFD is also significantly cheaper than RANS and many more cases can be run for the same computational budget. Therefore, the expected flight envelope can be sampled extensively using Euler CFD to get an initial drag polar set. Then, a small subset of this low-fidelity data is also evaluated with fine grid RANS CFD. In doing so, the high-fidelity RANS data augments the accuracy of the drag polars by accounting for viscous effects. The merging of these two datasets can be accomplished through a multi-fidelity surrogate modeling technique, specifically using Hierarchical Kriging [32].

For each of the BWB and TNW geometries, we generate a Latin hypercube design of experiments (DoE) on Mach and angle-of-attack containing 500 samples, which are evaluated using Euler CFD. Then, we select 35 points from this DoE based on how significantly they affect the predictions of the inviscid drag polar surrogate model. A uniform sampling on the expected Reynolds number range is then assigned to these 35 Mach and angle-of-attack combinations in a way that maximizes the distance between samples. The resulting DoE on Mach, angle-of-attack, and Reynolds number is then run in RANS CFD to obtain the viscous component of the multi-fidelity drag polars.

Once the Hierarchical Kriging surrogate models are created for each vehicle, we use the models to generate drag polar tables containing Mach, altitude, C_L, and C_D in a structured format, from sea-level all the way to 50,000 ft. These drag polars are then used by the mission analysis tool as lookup tables.

3.6 Engine Sizing and Cycle Selection

As mentioned previously, this study focuses on quantifying the airframe configuration change impact on the performance difference between the BWB and the TNW. As such, both vehicles need to have identical engines. The Boeing 767-300ER is powered by engines such as the CF6-80C2B7F1 and the PW4062 [15] with a sea-level-static (SLS) thrust of about 62,000 lb. For the BWB, the JetZero demonstrator is allegedly planning on using the PW2040 engine[6] with a SLS thrust of 40,000 lb[7]. Both the PW4062 and the PW2040 engines were introduced in the 1980s and thus are highly unlikely to feature on a 2030 variant of the TNW and BWB. If the 2030 time frame will have an aircraft fleet that is a mixture of both TNWs and BWBs for the 225 pax capacity, there is no off-the-shelf modern engine that can power both aircraft and thus a new engine will be required for these vehicles.

The PW2000 series engine comes in three thrust class variants: 37,000, 40,000, and 43,000 lb. Assuming engine manufacturers will target both the 2030 TNW and BWB aircraft with the same new engine for economic reasons, a 43,000 lb SLS thrust class engine seems like the best compromise. This engine should have more than enough thrust for the BWB, assuming the PW2040 is deemed adequate for the JetZero demonstrator. Although the SLS thrust rating is about 19,000 lb lower than the current engines powering the Boeing 767-300ER, it is expected that technological advancements

[6]Jon Ostrower, “JetZero Picks New Engine for USAF Demonstrator and Highlights a Void", The Air Current, July 11, 2024, last accessed July 17, 2024, https://theaircurrent.com/aircraft-development/jetzero-pw2040-blended-wing-ngas-demonstrator/

[7]“PW2000 Engine”, Pratt & Whitney, last accessed July 17, 2024, https://www.prattwhitney.com/en/products/commercial-engines/pw2000

of the 2030 engine will result in substantially higher fuel efficiency and thus lower fuel burn. The fuel weight savings will be augmented by reductions in engine weight from a reduced size and lighter materials. It is also reasonable to assume that the engine lapse rate will improve relative to 1980 levels resulting in substantially more thrust at higher altitudes. Thus, any climb and takeoff performance penalty that may occur by reducing the SLS thrust class for the TNW from 62,000 lb to 43,000 lb is likely to be offset, at least partially, by the improvements due to 2030 technology.

In the hypothetical scenario that an engine manufacturer is to develop a brand new engine in the 43,000 lb SLS thrust class for 2030, how would they go about doing so? To mimic such a development path, we assume that the logical starting point for this new engine would be the current state of the art in the nearest thrust class, which is the PW1133 geared turbofan. We believe that to obtain a 10,000 lb increase in SLS thrust, a new core and fan design is preferable, as a re-fan option, i.e., an increase in the fan size with the same core as the PW1133, may not be sufficient to produce the extra SLS thrust needed.

The notional engine model of the PW1133 is developed using the Numerical Propulsion System Simulation (NPSS) [33] code for engine cycle analysis and the WATE++ [34] code for engine weights and flow path estimation. We model the mechanical, thermodynamic, and geometric characteristics of this engine using public sources of information such as the European Union Aviation Safety Agency's ICAO engine emissions data bank [35] and type-certificate data sheet [36]. We use a multi-design point (MDP) process [37, 38] to design this engine given a set of requirements. The design points are: 1) the turbomachinery aerodynamic design point (ADP), where the cycle parameters are specified; 2) top of climb (TOC), which sets the maximum mass flow and corrected speed, and thus sizes the fan; 3) hot day takeoff (TKO) where the maximum temperature conditions is established; 4) SLS installed and 5) SLS uninstalled where the sea level static thrust target is specified.

With the baseline model established, we select a few design characteristics to perturb and model a realistic set of changes that would be achievable in the next six years. Table 1 presents the differences between the current notional PW1133 engine model to a 2030 variant with higher SLS thrust. Additional design characteristics of this engine are presented in Table 4 in Sec. 4.2. We decided on a larger fan with a lower FPR, thereby increasing the BPR. We also increased the OPR and maximum combustor exit temperature to allow for the generation of more thrust. Lastly, we also decreased the lapse rate of the engine by 5% assuming that by 2030, the thrust loss at higher altitudes will be lower. We define the lapse rate in this context as the ratio of the top-of-climb thrust to the uninstalled sea-level-static thrust. Figure 6 presents the 2030 engine architecture, featuring a three-stage low-pressure compressor, an eight-stage high-pressure compressor, a two-stage high-pressure turbine, and a three-stage low-pressure turbine.

In an idealized scenario, both aircraft would have potentially different engines that best match the airframe they power. In fact, the initial 800pax BWB design showed a 27% reduction in the thrust requirement [6] whereas the BWB-450 showed a 19% reduction in thrust [7] relative to the reference TNW aircraft. It is therefore reasonable to assume that the optimum engines for each vehicle will end

Table 1 – Comparison between the notional PW1133 geared turbofan and the 2030 upgraded variant with higher SLS thrust

	Notional PW1133	2030 Engine
Aero Design Point (ADP)	Mach 0.85 at 39,000 ft	Mach 0.85 at 39,000 ft
Fan Pressure Ratio (FPR) at ADP	1.52	1.45
Overall Pressure Ratio (OPR) at ADP	45.8	52
Bypass Ratio (BPR) at ADP	11.7	13.5
Fan Diameter (in)	80.5	99.5
Max Combustor Exit Temp (°R)	3360	3400
Uninstalled Sea Level Static Thrust (lb)	33,110	43,000
Lapse Rate	0.1842	0.1934

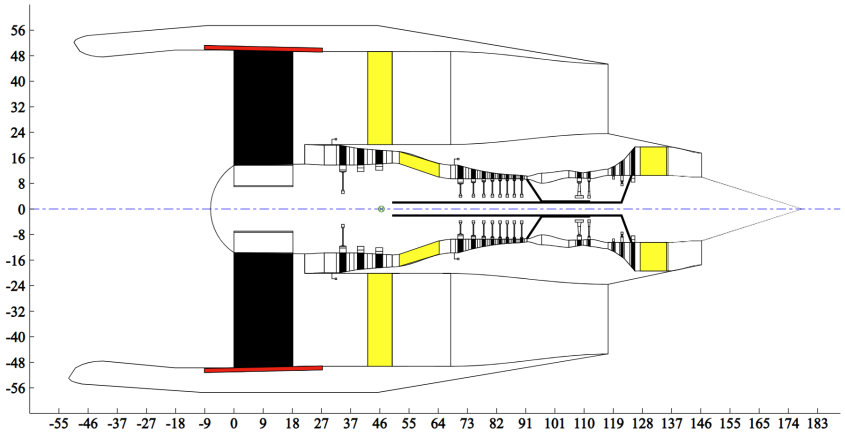

Figure 6 – WATE++ output of the 2030 engine architecture (axes represent dimension in inches)

up with different thrust levels and cycle designs. To ascertain the performance difference between the BWB and TNW in such a scenario, we also conduct a cycle optimization exercise. Table 2 shows the engine design variables and their ranges considered for this study, starting with the notional PW1133 engine model. We prepared a 5,000 case DoE that samples this design space, and then for every engine design perturbation, we sized the vehicles and ran a mission analysis. We tracked the mission block fuel burn, the resulting fan diameter of the engine, and the combustor inlet temperature. We set a maximum limit on the fan constraint to 99.5 inches for both vehicles, the same as the 43,000 lb thrust class engine, to account for ground clearance limits for the TNW and aerodynamic performance limits on the BWB. We also set an upper limit on the combustor inlet total temperature to 1,800 °R. We then picked the engine designs that had the lowest fuel burn while satisfying the constraints. These designs are presented in Sec. 4.3.

Table 2 – Cycle optimization variables and bounds, starting with the notional PW1133 engine model

Variable	Lower Bound	Upper Bound
FPR at ADP	1.40	1.55
OPR at ADP	45	60
Max Combustor Exit Temperature (°R)	3,300	3,400
Engine SLS Thrust to Aircraft Gross Weight Ratio	0.25	0.35

3.7 System Analysis

We use FLOPS [39] to model the system-level performance of the BWB and TNW. We integrate the propulsion system performance into FLOPS through engine decks that contain fuel flow rate and net thrust at different Mach-altitude combinations for varying engine throttle settings. As discussed in Sec. 3.5, CFD-generated drag polars are used for the aerodynamics component of the tool, but these do not include the nacelles and pylons in the model. Therefore, we use FLOPS empirical relations to estimate the nacelle drag addition, which is a function of the length, max diameter, and flight conditions. We then add a small constant amount of parasitic drag for the pylons and excrescence.

The notional profiles for the primary and reserve missions for both the BWB and TNW are shown in Fig. 7. The climb segment is optimized for minimum time to climb in FLOPS. The cruise climb segment for the design mission is optimized for a specific range, whereas the descent segment is run at the maximum vehicle L/D. The start and end of cruise altitudes for the primary mission are a fallout of the converged aircraft weight, SLS thrust, engine lapse rate, and aerodynamic performance. We specify a design mission range of 5,000 nmi, with a reserve mission range of 200 nmi to an alternate airport. The reserve mission also includes a 30 minute hold at 1,500 ft altitude and Mach 0.4. The

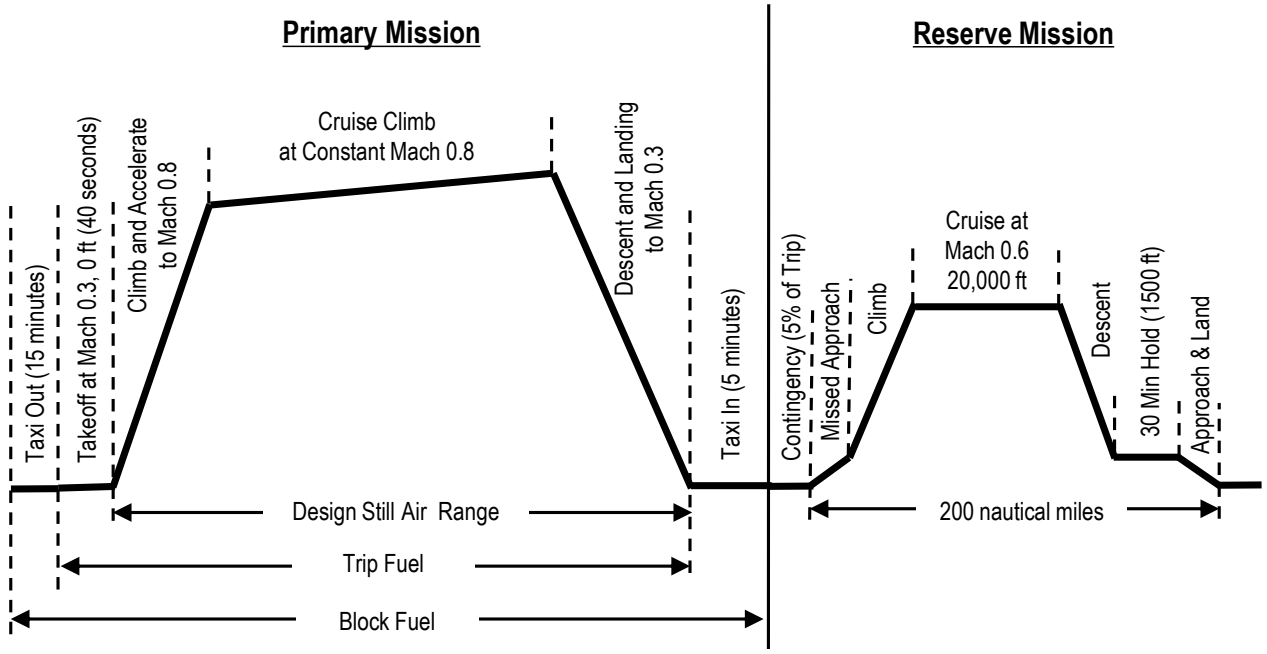

Figure 7 – Notional mission profile for the BWB and TNW

total reserve fuel is the value required to fly the reserve mission plus an additional 5% of the trip fuel for contingencies. We also evaluate the primary mission profile for a 900 nmi range to represent an economic mission. The economic mission is paired with the same reserve mission as the design mission case. The design payload is 225 passengers, assuming a 250 lb weight per passenger including baggage, for a total of 56,250 lb. We also assume a total of six flight attendants (roughly one per 40 passengers) and two pilots for both aircraft.

We use FLOPS internal weight equations for predicting the structural weight and most of the other non-structural operating empty weight components. WATE++ is used to compute the propulsion weights. For the BWB, the default FLOPS assumption is a composite centerbody and a metal outboard wing and aft body. However, we instead assume a pultruded rod, stitched, efficient, unitized structure (PRSEUS) centerbody and aft-body, and a conventional composite outboard wing. The specified weight savings from PRSEUS and conventional composite technologies relative to the default FLOPS assumptions are indicated in Fig. 8. FLOPS has wing and centerbody weight calibration factors, i.e., FRWI 1-4 and FRFU respectively, that can correct the weight predictions from its internal equations. The values of these factors are adjusted to reflect the assumed weight benefits of conventional composites and PRSEUS. The weight savings factors are derived from the nominal values for the final milestone in previous work associated with NASA Environmentally Responsible Avia-

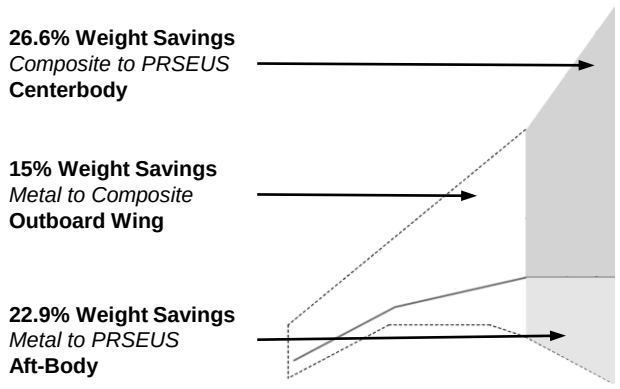

Figure 8 – Assumed weight savings going from FLOPS default assumptions to applied material technologies

tion Integrated Technology Demonstrations (ERA ITDs), documented in [40]. We assume a weight savings of 15% when considering baseline composites over a conventional metallic structure. Additionally, the weight reduction values of PRSEUS compared to baseline composites are multiplicative. For example, the ERA ITD study shows a weight savings of 9.3% using PRSEUS instead of baseline composites for the aft body. Assuming the 15% savings from metal to baseline composite, the cumulative weight savings going from metal to PRSEUS is 22.9%.

As mentioned previously, we model two variants of the TNW with different structural materials. The first, a "conventional" TNW, is intended to represent an older airframe that is still in service by 2030, but will be re-engined for better efficiency, As such, this airframe still has a metallic structure. The second version is an "advanced" TNW with composites for the wing and fuselage. This variant is reflective of a more modern airframe that is likely to be flown in the 2030 time frame. For the advanced TNW, we assume a 15% savings on the fuselage and wing weight relative to FLOPS predictions, which by default assume metallic structures. For the BWB and TNW, all other weight scaling factors in FLOPS were left at their default values.

4 Results and Discussion

4.1 Optimization Results and Cruise Performance Comparison

Figure 9 compares the baseline and optimized BWB aerodynamic performance at Mach 0.8 at an altitude of 40,000 ft, whereas Fig. 10 does the same for the TNW. For the BWB, optimization improves the peak L/D from 23.8 to 25.2, a roughly 6% increase relative to the baseline. For the TNW, the difference in the maximum L/D between the two is rather small, with a peak L/D of 21.95 at a C_L of 0.497 for the optimized configuration and a peak L/D of 21.89 at a C_L of 0.504 for the baseline. The small improvement in peak L/D after optimization for the TNW can likely be attributed to the preliminary work done in improving the twist distribution of the baseline geometry relative to the CRM twist, as mentioned in Sec. 3.2. For both the BWB and TNW, there is a consistent downward shift in the lift curve for the optimized configuration relative to the baseline, albeit smaller for the TNW. This result is primarily a consequence of the increased downward twist of the outboard wing root section for the BWB and the increased downward twist past the 45% span-wise location for the TNW. Note that these results do not include any contributions for nacelle, pylon, interference and excrescence drag. The clean optimized BWB airframe at these flight conditions exhibits a 15% higher peak L/D compared to the clean optimized TNW airframe.

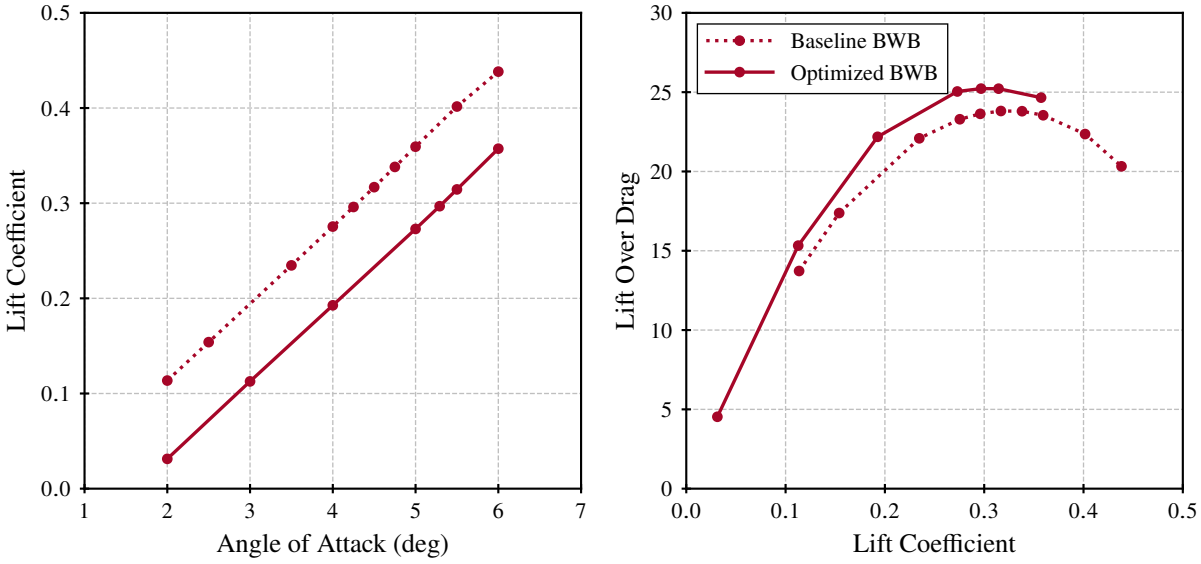

Figure 9 – Comparison of the lift curve and lift-over-drag for the baseline and optimized BWB configurations (does not include nacelle, pylon, and excrescence drag)

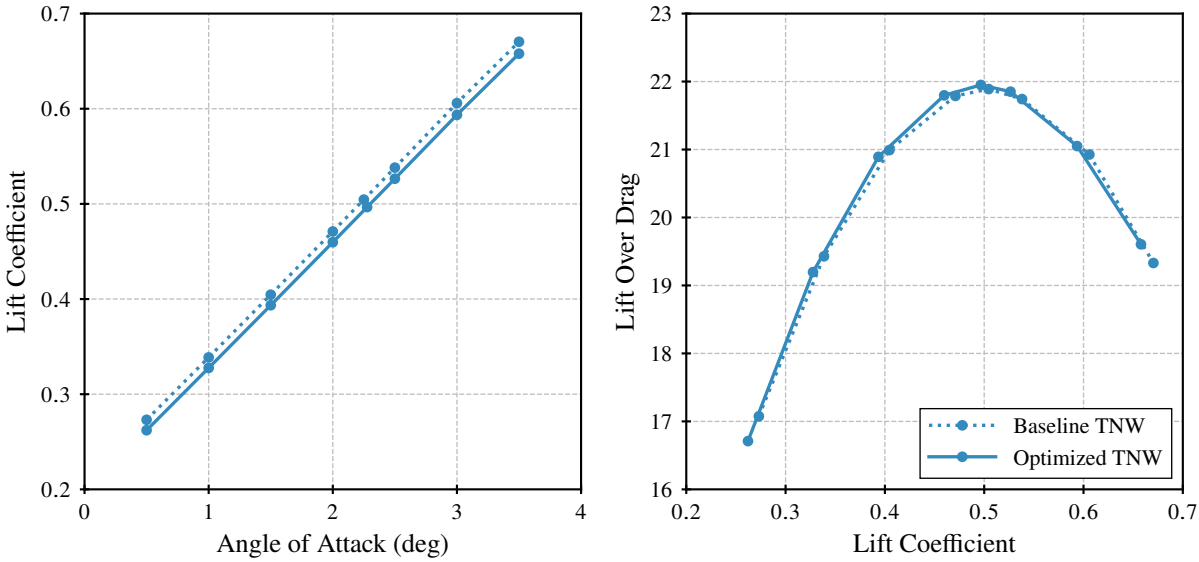

Figure 10 – Comparison of the lift curve and lift-over-drag for the baseline and optimized TNW configurations (does not include nacelle, pylon, and excrescence drag)

4.2 Mission Performance Comparison (Same Engine)

This section provides different quantitative metrics for comparing the configuration change impact on the performance difference between the BWB and the TNW powered by the same engine. Table 3 compares the system level performance for the design, economic, and associated reserve missions. The performance characteristics at the different engine design points of the common engine powering both configurations are detailed in Table 4. For this engine, ADP and TOC are defined at Mach 0.85, 39,000 ft whereas TKO is at Mach 0.25, sea-level, with a $+27^{\circ}$R deviation from standard atmosphere.

Table 3 – Comparison of the system level results for the design and reserve, and economic and reserve missions for the same engine case

	BWB		TNW (Metal)		TNW (Composites)	
	Design	Reserve	Design	Reserve	Design	Reserve
Range (nmi)	5,000	200	5,000	200	5,000	200
Cruise Mach	0.8	0.6	0.8	0.6	0.8	0.6
SOC Alt. (ft)	43,203	20,000	37,491	20,000	38,466	20,000
EOC Alt. (ft)	47,175	20,000	42,063	20,000	42,979	20,000
Cruise L/D Range	22.9-23.2	N/A	19.2-19.8	N/A	19.1-19.7	N/A
Fuel Burn (lb)	60,999	9,650	80,180	11,587	76,639	11,267
Payload (lb)	56,250		56,250		56,250	
Operating Empty Wt. (lb)	143,125		169,668		156,211	
Ramp Weight (lb)	270,024		317,685		300,367	
	Economic	Reserve	Economic	Reserve	Economic	Reserve
Range (nmi)	900	200	900	200	900	200
Cruise Mach	0.8	0.6	0.8	0.6	0.8	0.6
SOC Alt. (ft)	46,942	20,000	41,759	20,000	42,689	20,000
EOC Alt. (ft)	47,372	20,000	42,281	20,000	43,211	20,000
Cruise L/D Range	22.8-22.9	N/A	19.2-19.3	N/A	19.0-19.1	N/A
Fuel Burn (lb)	11,815	7,191	14,703	8,312	14,118	8,142
Payload (lb)	56,250		56,250		56,250	
Operating Empty Wt. (lb)	143,125		169,668		156,211	
Ramp Weight (lb)	218,381		248,933		234,722	

Table 4 – Design characteristics of the 43,000 lb thrust class common engine used for the BWB and the TNW aircraft

Engine Length (in)	147	SLS Thrust (lb)	43,000
Fan Diameter (in)	99.5	SLS TSFC (lbm/lbf-hr)	0.2398
ADP FPR	1.45		
ADP LPCPR	2.14	TKO Thrust (lb)	34,644
ADP HPCPR	17.0	TKO TSFC (lbm/lbf-hr)	0.3505
ADP OPR	52.0		
ADP BPR	13.5	TOC Thrust (lb)	8,318
ADP Thrust (lb)	7,908	TOC TSFC (lbm/lbf-hr)	0.5317
ADP TSFC (lbm/lbf-hr)	0.5275		

For the design mission, the BWB shows a 17-18% higher peak operating cruise L/D compared to the TNW variants. Correspondingly, the BWB design mission fuel burn is 24% lower than the TNW with metallic structures and 20% lower than the TNW composites reference aircraft. The ramp weight of the BWB is also lighter, showing a 15% reduction over the TNW metal variant and a 10% reduction over the TNW composite reference case. Since both aircraft are powered by the same engine, the lighter and more aerodynamically efficient BWB can operate at higher altitudes compared to the TNW reference aircraft. Note that the BWB start of cruise (SOC) altitude is higher than the end of cruise (EOC) altitude of both TNW variants. The high cruise altitudes also suggest that this BWB model may not need a 43,000 lb SLS thrust engine. Lower fuel burn can likely be achieved for the BWB by downsizing the engine, albeit at the cost of takeoff performance, which was not modeled.

For the economic mission, the BWB shows a 19-20% improvement in operating cruise L/D, but only a 16-20% improvement in fuel burn and a 7-12% reduction in ramp weight relative to the TNW variants. Coupled with the 5,000 nmi design mission results, these findings suggest that the efficiency of the BWB relative to the TNW tends to improve for longer mission ranges.

Table 5 compares the detailed component weight breakdowns. The lower operating empty weight of the BWB over the TNW largely stems from the reduced structural weight. PRSEUS is a key enabling technology in reducing the BWB airframe weight, and the lack of empennage for the BWB is also beneficial. The lower ramp weight also means that the landing gear for the BWB does not have to be as heavy as the TNW landing gear. The systems and equipment weight and operating items weight are similar for all three variants. As such, the reduced fuel burn for the BWB is due to the superior aerodynamic efficiency and the lighter structural weight of the airframe compared to the TNW.

The BWB and TNW performance differences quoted above are comparable to those published in the literature, as presented in the introduction. In particular, these performance changes are only a few percent lower than Liebeck et al. [6, 7] numbers on the configuration change benefit. The much higher 50% and 60% fuel burn savings numbers quoted by DZYNE and JetZero, as mentioned in the introduction, are against reference TNW aircraft with older technology levels, in particular, the engines. Since we deliberately enforce the same engine constraint in our comparison, the engine technology benefits are not a factor in our fuel burn differences.

4.3 Mission Performance Comparison (Different Optimized Engines)

If we relax our previous assumptions and allow the 2030 technology-level engines for both the TNW and BWB to re-size while optimizing the cycle to best pair the engine with a given configuration, what do the performance differences look like in this scenario? Table 6 compares the system-level performance for the design, economic, and associated reserve missions. The performance characteristics for the three re-sized and optimized engines are detailed in Tables 7, 8, and 9. The design points for these three engines are the same as before. The TNW variants share the same cycle, but the engine thrust was allowed to re-scale based on the aircraft ramp weight.

Table 5 – Detailed weight breakdown comparison between the BWB and TNW for the design plus reserve missions for the common 43,000 lb engine case

Weight Component	BWB (lb)	TNW Metal (lb)	TNW Composite (lb)
Outboard Wing	19,283	36,373	29,703
Winglet	568	858	717
Centerbody	39,473	38,598	32,808
Horizontal Tail	0	4,252	4,205
Vertical Tail	0	1,705	1,676
Landing Gear	9,407	12,547	11,874
Structures Total	*68,731*	*94,333*	*80,983*
Engine Components (incl. nacelle/pylon)	24,408	24,408	24,408
Fuel System Tanks and Plumbing	918	1,060	1,024
Propulsion Total	*25,326*	*25,468*	*25,432*
Surface Controls	1,441	3,764	3,697
APU	1,282	1,298	1,298
Instruments	714	710	710
Hydraulics	2,500	2,178	2,178
Electrical	2,161	2,481	2,481
Avionics	1,787	1,859	1,859
Furnishings and Equipment	26,936	25,187	25,187
Air Conditioning	2,434	2,662	2,662
Anti-Icing	332	279	279
Systems and Equipment Total	*39,587*	*40,418*	*40,351*
Crew and Baggage	1,650	1,650	1,650
Unusable Fuel	855	702	698
Engine Oil	168	168	168
Passenger Service	4,680	4,801	4801
Cargo Containers	2,128	2,128	2128
Additional Operating Items Total	*9,481*	*9,449*	*9,445*
Payload Total (225 pax @250 lb/pax)	*56,250*	*56,250*	*56,250*
Design Mission Fuel	60,999	80,180	76,639
Reserve Mission Fuel	9,650	11,587	11,267
Fuel Total	*70,649*	*91,767*	*87,906*
Ramp Weight	*270,024*	*317,685*	*300,367*

Table 6 – Comparison of the system level results for the design and reserve missions, and economic and reserve missions for the different optimized engines case

	BWB		TNW (Metal)		TNW (Composites)	
	Design	Reserve	Design	Reserve	Design	Reserve
Range (nmi)	5,000	200	5,000	200	5,000	200
Cruise Mach	0.8	0.6	0.8	0.6	0.8	0.6
SOC Alt. (ft)	40,280	20,000	35,995	20,000	35,716	20,000
EOC Alt. (ft)	43,981	20,000	40,384	20,000	40,059	20,000
Cruise L/D Range	22.1-22.8	N/A	18.9-19.6	N/A	18.4-19.3	N/A
Fuel Burn (lb)	59,546	9,054	78,976	11,205	75,766	10,769
Payload (lb)	56,250		56,250		56,250	
Operating Empty Wt. (lb)	138,999		166,684		151,632	
Ramp Weight (lb)	263,849		313,115		294,417	
	Economic	Reserve	Economic	Reserve	Economic	Reserve
Range (nmi)	900	200	900	200	900	200
Cruise Mach	0.8	0.6	0.8	0.6	0.8	0.6
SOC Alt. (ft)	43,757	20,000	40,052	20,000	39,716	20,000
EOC Alt. (ft)	44,163	20,000	40,619	20,000	40,299	20,000
Cruise L/D Range	22.1-22.2	N/A	18.9-19.0	N/A	18.4-18.5	N/A
Fuel Burn (lb)	11,316	6,643	14,371	7,975	13,724	7,666
Payload (lb)	56,250		56,250		56,250	
Operating Empty Wt. (lb)	138,999		166,684		151,632	
Ramp Weight (lb)	213,208		245,280		229,272	

Table 7 – Design characteristics of the optimized and re-sized engine for the BWB configuration

Engine Length (in)	137	SLS Thrust (lb)	36,149
Fan Diameter (in)	94.9	SLS TSFC (lbm/lbf-hr)	0.2323
ADP FPR	1.41	SLS Thrust/Ramp Weight	0.2740
ADP LPCPR	2.44	TKO Thrust (lb)	29,124
ADP HPCPR	17.0	TKO TSFC (lbm/lbf-hr)	0.3451
ADP OPR	57.6		
ADP BPR	14.2	TOC Thrust (lb)	6,993
ADP Thrust (lb)	6,647	TOC TSFC (lbm/lbf-hr)	0.5271
ADP TSFC (lbm/lbf-hr)	0.5240		

Table 8 – Design characteristics of the optimized and re-sized engine for the TNW metal configuration

Engine Length (in)	140	SLS Thrust (lb)	39,230
Fan Diameter (in)	95.9	SLS TSFC (lbm/lbf-hr)	0.2365
ADP FPR	1.44	SLS Thrust/Ramp Weight	0.2506
ADP LPCPR	2.44	TKO Thrust (lb)	31,606
ADP HPCPR	17.0	TKO TSFC (lbm/lbf-hr)	0.3472
ADP OPR	58.9		
ADP BPR	13.3	TOC Thrust (lb)	7,589
ADP Thrust (lb)	7,210	TOC TSFC (lbm/lbf-hr)	0.5287
ADP TSFC (lbm/lbf-hr)	0.5247		

Table 9 – Design characteristics of the optimized and re-sized engine for the TNW composite configuration

Engine Length (in)	137	SLS Thrust (lb)	36,888
Fan Diameter (in)	93	SLS TSFC (lbm/lbf-hr)	0.2368
ADP FPR	1.44	SLS Thrust/Ramp Weight	0.2506
ADP LPCPR	2.44	TKO Thrust (lb)	29,719
ADP HPCPR	17.0	TKO TSFC (lbm/lbf-hr)	0.3480
ADP OPR	58.9		
ADP BPR	13.2	TOC Thrust (lb)	7,136
ADP Thrust (lb)	6,780	TOC TSFC (lbm/lbf-hr)	0.5306
ADP TSFC (lbm/lbf-hr)	0.5266		

In general, the performance differences between the BWB and TNW are similar or slightly better than those in the same engine comparison. For the design mission, the BWB shows a 16-18% higher peak operating cruise L/D compared to the TNW variants. The BWB design mission fuel burn is 25% lower than the TNW metal variant and 21% lower than the TNW composites reference aircraft. The ramp weight of the BWB is still lighter, showing a 16% reduction over the TNW metal variant and a 10% reduction over the TNW composite reference case. For the economic mission, the BWB shows a 17-20% improvement in operating cruise L/D, a 17-21% improvement in fuel burn, and a 7-13% reduction in ramp weight relative to the TNW variants.

All three vehicles favor smaller thrust class engines, which results in a reduction in their operating cruise altitude. Compared to the TNW metal configuration, the BWB shows an 8% reduction in SLS thrust, which drops to 2% relative to the TNW composite configuration. The length and diameter of all three engines are smaller than the common engine used previously. As expected, optimization decreased FPR and increased OPR, resulting in a lower thrust-specific fuel consumption (TSFC) for all three engines at all design points compared to the common engine.

Table 10 compares the detailed component weight breakdowns. All three vehicles have a lower operating weight as a consequence of the lighter engines. The other component weight changes relative to the previous scenario are a consequence of re-sizing the airframes for the new engines.

Although not part of the original problem scope, it is still informative to compare the total fuel required for the BWB design and reserve mission to the currently flying variants in the Boeing 767 family, with existing engines, for the same payload and range requirements. Sections 3.2.1 to 3.2.4 in Ref. [15] show the payload-range diagrams for the Boeing 767-200, 200ER, 300, and 300ER respectively. The Boeing 767-200 cannot fly the design payload-range point considered previously in this study. As such, we had to determine another common point to compare the aircraft performance. The payload-range diagram for the 767-200 quotes an operating empty weight of 176,100 lb. As a crude approximation, we assume this operating empty weight is the same regardless of range. The sum of the operating empty weight and payload is also provided in this diagram from which we can estimate the payload to be 43,564 lb. The maximum range that can be flown for this particular payload and empty weight is estimated to be 3,923 nmi with a maximum design taxi weight (ramp weight) of 317,000 lb. We then estimated the maximum design taxi weights for the other 767 variants from their respective diagrams for the 43,564 lb payload and 3.923 nmi range pair. The total fuel weight is then calculated as the maximum design taxi weight minus the operating empty weight and payload. Table 11 compares the BWB with the 43,000 lb SLS thrust engine to the Boeing 767 variants. The BWB's overall 43-52% fuel savings over the 767 family is consistent with JetZero's publicly quoted fuel burn savings for their BWB. In this instance, it is both the airframe and 2030 engine upgrades on the BWB, relative to the existing 767s, that contribute towards this larger fuel savings.

Table 10 – Detailed weight breakdown comparison between the BWB and TNW for the design plus reserve missions for the optimized engines case

Weight Component	BWB (lb)	TNW Metal (lb)	TNW Composite (lb)
Outboard Wing	19,012	36,053	29,360
Winglet	564	854	713
Centerbody	39,317	38,598	32,808
Horizontal Tail	0	4,240	4,188
Vertical Tail	0	1,697	1,666
Landing Gear	9,214	12,383	11,625
Structures Total	*68,107*	*93,825*	*80,360*
Engine Components (incl. nacelle/pylon)	20,944	21,965	20,502
Fuel System Tanks and Plumbing	918	1,060	1,024
Propulsion Total	*21,862*	*23,025*	*21,526*
Surface Controls	1,430	3,746	3,673
APU	1,282	1,298	1,298
Instruments	7,14	710	710
Hydraulics	2,500	2,178	2,178
Electrical	2,161	2,481	2,481
Avionics	1,787	1,859	1,859
Furnishings and Equipment	26,936	25,187	25,187
Air Conditioning	2,434	2,662	2,662
Anti-Icing	328	276	274
Systems and Equipment Total	*39,572*	*40,397*	*40,322*
Crew and Baggage	1,650	1,650	1,650
Unusable Fuel	840	699	692
Engine Oil	151	159	153
Passenger Service	4,680	4,801	4,801
Cargo Containers	2,128	2,128	2,128
Additional Operating Items Total	*9,458*	*9,437*	*9,424*
Payload Total (225 pax @250 lb/pax)	*56,250*	*56,250*	*56,250*
Design Mission Fuel	59,546	78,976	75,766
Reserve Mission Fuel	9,054	11,205	10,769
Fuel Total	*68,600*	*90,181*	*86,535*
Ramp Weight	*263,849*	*313,115*	*294,417*

Table 11 – Comparison of the BWB to the Boeing 767 family for a 3,923 nmi mission range and a 43,564 lb payload

	BWB	B767-200	B767-200ER	B767-300	B767-300ER
Payload (lb)	43,564	43,564	43,564	43,564	43,564
Range (nmi)	3,923	3,923	3,923	3,923	3,923
Operating Empty Weight (lb)	143,125	176,100	182,900	187,900	187,900
Ramp Weight (lb)	240,403	317,000	321,000	334,000	343,000
Total Fuel Weight (lb)	53,714	97,336	94,536	102,536	111,536
BWB Fuel Savings vs. TNW		45%	43%	48%	52%

5 Conclusions

This study aimed to quantify the benefit of the BWB configuration over the TNW. To ensure an apples-to-apples comparison, both aircraft were designed to carry 225 passengers and fly a 5,000 nmi design mission range. A reserve mission with a 200 nmi range to an alternate airport was also included. Both aircraft used the same engines, designed for a 2030 time frame with a 43,000 lb SLS thrust. Starting with internally developed parametric geometry models, we optimized both the BWB and TNW using CFD simulations, multi-fidelity techniques, and gradient-free approaches. We then used CFD to generate a set of drag polars spanning the flight envelope for both the BWB and TNW to use with our mission analysis. We also performed a second comparison where the engines for the BWB and TNW were allowed to re-size while optimizing the engine cycle for each configuration. We modeled two variants of the TNW, one with metallic structures and one that uses composites. Figure 11 summarizes the design mission performance differences between the BWB and TNW for these two comparisons. Our results demonstrate that the BWB airframe outperforms the TNW configuration, with the primary benefits stemming from the aerodynamically superior and structurally lighter airframe.

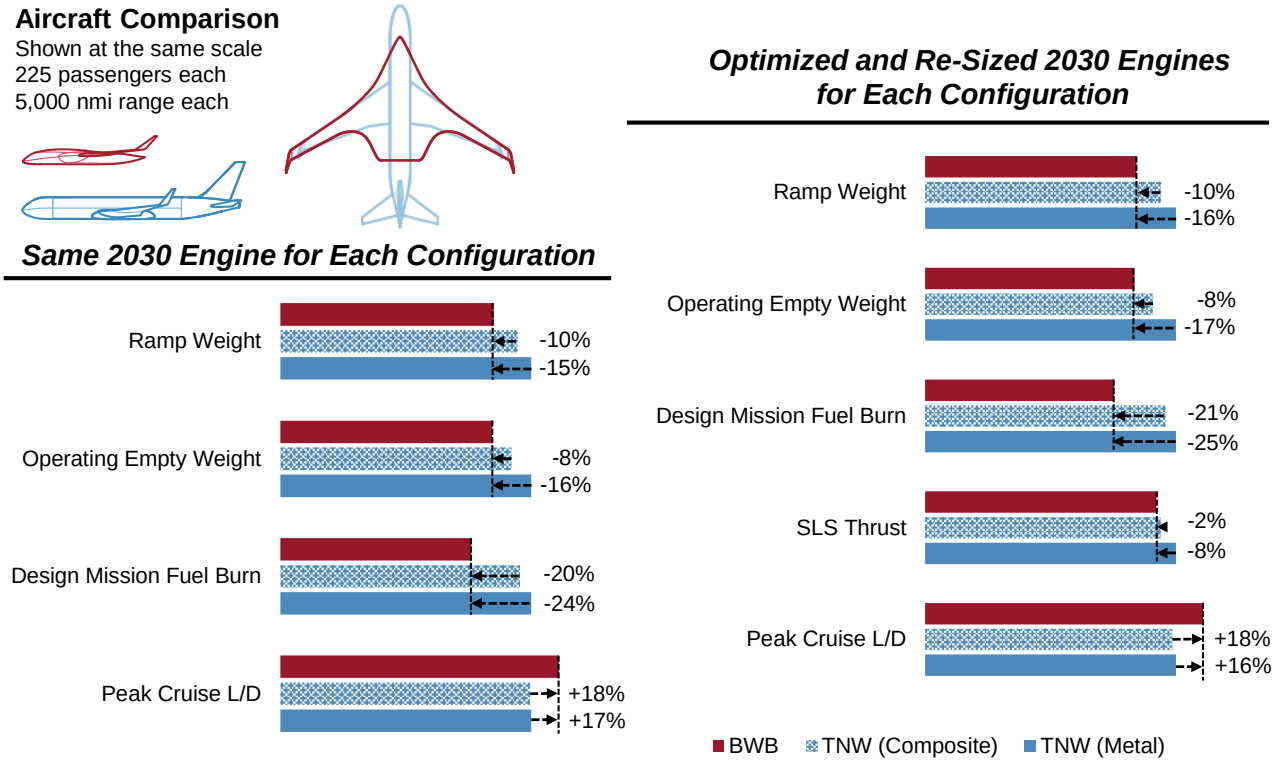

Figure 11 – Summary of the performance differences between the BWB and the TNW for the design mission, for the same and different engine cases

6 Contact Author Email Address

Corresponding author: Jimmy Tai (jimmy.tai@ae.gatech.edu)

7 Copyright Statement

References

[1] International Air Transport Association. Fact sheet: Climate change & CORSIA. A40-WP/54, IATA, 2019.

[2] John R. Hooker and Andrew T. Wick. Design of a hybrid wing body for fuel efficient air mobility operations at transonic flight conditions. In *52nd Aerospace Sciences Meeting*. American Institute of Aeronautics and Astronautics, January 2014.

[3] Andrew T. Wick, John R. Hooker, Casie M. Clark, Ryan Plumley, and Cale Zeune. Powered low speed testing of the hybrid wing body. In *55th AIAA Aerospace Sciences Meeting*. American Institute of Aeronautics and Astronautics, January 2017.

[4] Yueping Guo, Casey L. Burley, and Russell H. Thomas. On noise assessment for blended wing body aircraft. In *52nd Aerospace Sciences Meeting*. American Institute of Aeronautics and Astronautics, January 2014.

[5] Cesare A. Hall and Daniel Crichton. Engine design studies for a silent aircraft. *Journal of Turbomachinery*, 129(3):479–487, 07 2006.

[6] Robert Liebeck, Mark Page, and Blaine Rawdon. Blended-wing-body subsonic commercial transport. In *36th AIAA Aerospace Sciences Meeting and Exhibit*. American Institute of Aeronautics and Astronautics, January 1998.

[7] Robert H. Liebeck. Design of the blended wing body subsonic transport. *Journal of Aircraft*, 41(1):10–25, January 2004.

[8] James Hileman, Zoltan Spakovszky, Mark Drela, and Matthew Sargeant. Airframe design for "silent aircraft". In *45th AIAA Aerospace Sciences Meeting and Exhibit*. American Institute of Aeronautics and Astronautics, January 2007.

[9] Ronald T. Kawai. Acoustic prediction methodology and test validation for an efficient low-noise hybrid wing body subsonic transport. Technical Report NF1676L-14465, NASA, February 2011.

[10] Malcom Brown and Roelof Vos. Conceptual design and evaluation of blended-wing body aircraft. In *2018 AIAA Aerospace Sciences Meeting*. American Institute of Aeronautics and Astronautics, January 2018.

[11] Shanling Yang, Mark Page, and Ed J. Smetak. Achievement of NASA new aviation horizons N+2 goals with a blended-wing-body X-plane designed for the regional jet and single-aisle jet markets. In *2018 AIAA Aerospace Sciences Meeting*. American Institute of Aeronautics and Astronautics, January 2018.

[12] Mark Page, Ed J. Smetak, and Shanling Yang. Single-aisle airliner disruption with a single-deck blended-wingbody. In *31st Congress of the International Council of the Aeronautical Sciences*. International Council of the Aeronautical Sciences, 2018.

[13] Robert Haimes and John Dannenhoffer. The engineering sketch pad: A solid-modeling, feature-based, web-enabled system for building parametric geometry. In *21st AIAA Computational Fluid Dynamics Conference*, Reston, Virginia, jun 2013. American Institute of Aeronautics and Astronautics.

[14] Brenda M. Kulfan. Universal parametric geometry representation method. *Journal of Aircraft*, 45(1):142–158, 2008.

[15] Boeing Commerical Airplanes. *767 Airplane Characteristics for Airport Planning*, August 2023. Rev. J.

[16] John Vassberg, Mark Dehaan, Melissa Rivers, and Richard Wahls. Development of a common research model for applied CFD validation studies. In *26th AIAA Applied Aerodynamics Conference*. American Institute of Aeronautics and Astronautics, June 2008.

[17] O. Atinault and D. Hue. Design of a vertical tail for the CRM configuration. Technical Report RT 1/21960 GMT/DAAP, ONERA, June 2014.

[18] Meng-Sing Liou. A sequel to AUSM: AUSM+. *Journal of Computational Physics*, 129(2):364–382, 1996.

[19] Venkat Venkatakrishnan. Convergence to steady state solutions of the Euler equations on unstructured grids with limiters. *Journal of Computational Physics*, 118(1):120–130, 1995.

[20] Florian R. Menter. Improved two-equation $k-\omega$ turbulence models for aerodynamic flows. Technical Memorandum NASA-TM-103975, NASA, October 1992.

[21] Jai Ahuja, Chung Hyun Lee, Christian Perron, and Dimitri N Mavris. Comparison of overwing and underwing nacelle aeropropulsion optimization for subsonic transport aircraft. *Journal of Aircraft*, 61(2):638–653, mar 2024.

[22] Donald R Jones, Matthias Schonlau, and J William. Efficient global optimization of expensive black-box functions. *Journal of Global Optimization*, 13:455–492, 1998.

[23] Alexander I. J. Forrester, András Sóbester, and Andy J. Keane. *Engineering Design via Surrogate Modelling: A Practical Guide*. Wiley, July 2008.

[24] David Ginsbourger, Rodolphe Le Riche, and Laurent Carraro. *Kriging Is Well-Suited to Parallelize Optimization*, page 131–162. Springer Berlin Heidelberg, 2010.

[25] Patrick N. Koch, Timothy W. Simpson, Janet K. Allen, and Farrokh Mistree. Statistical approximations for multidisciplinary design optimization: The problem of size. *Journal of Aircraft*, 36(1):275–286, January 1999.

[26] Sushma Kumari and Balasubramaniam Jayaram. Measuring concentration of distances—an effective and efficient empirical index. *IEEE Transactions on Knowledge and Data Engineering*, 29(2):373–386, February 2017.

[27] Paul G. Constantine, Eric Dow, and Qiqi Wang. Active subspace methods in theory and practice: Applications to Kriging surfaces. *SIAM Journal on Scientific Computing*, 36(4):A1500–A1524, January 2014.

[28] Dushhyanth Rajaram, Raphael H. Gautier, Christian Perron, Olivia J. Pinon-Fischer, and Dimitri Mavris. Non-intrusive parametric reduced order models with high-dimensional inputs via gradient-free active subspace. In *AIAA AVIATION 2020 FORUM*. American Institute of Aeronautics and Astronautics, June 2020.

[29] Raphaël Gautier, Piyush Pandita, Sayan Ghosh, and Dimitri Mavris. A fully Bayesian gradient-free supervised dimension reduction method using Gaussian processes. *International Journal for Uncertainty Quantification*, 12(2):19–51, 2022.

[30] Bilal Mufti, Mengzhen Chen, Christian Perron, and Dimitri N. Mavris. A multi-fidelity approximation of the active subspace method for surrogate models with high-dimensional inputs. In *AIAA AVIATION 2022 Forum*, pages 1–26, Reston, Virginia, June 2022. American Institute of Aeronautics and Astronautics.

[31] R. C. Feagin and W. D. Morrison. Delta method, an empirical drag buildup technique. Contractor Report NASA-CR-151971, NASA, December 1978.

[32] Zhong-Hua Han and Stefan Görtz. Hierarchical Kriging model for variable-fidelity surrogate modeling. *AIAA Journal*, 50(9):1885–1896, September 2012.

[33] John K. Lytle. The numerical propulsion system simulation: A multidisciplinary design system for aerospace vehicles. Technical Memorandum NASA/TM-1999-209194, NASA, 1999.

[34] Michael T. Tong and Bret A. Naylor. An object-oriented computer code for aircraft engine weight estimation. In *Volume 1: Aircraft Engine; Ceramics; Coal, Biomass and Alternative Fuels; Manufacturing, Materials and Metallurgy; Microturbines and Small Turbomachinery*, GT2008. ASMEDC, January 2008.

[35] European Union Aviation Safety Agency. ICAO aircraft engine emissions databank, July 2024. Data retrieved from https://www.easa.europa.eu/en/domains/environment/icao-aircraft-engine-emissions-databank.

[36] International Aero Engines (IAE), LLC. PW1100G-JM series engines. Type-Certificate Data Sheet IM.E.093, EASA, October 2022.

[37] Jeffrey Schutte, Jimmy Tai, Jonathan Sands, and Dimitri Mavris. Cycle design exploration using multi-design point approach. In *Volume 1: Aircraft Engine; Ceramics; Coal, Biomass and Alternative Fuels; Controls, Diagnostics and Instrumentation*, GT2012. American Society of Mechanical Engineers, June 2012.

[38] Jeffrey Schutte. *Simultaneous Multi-Design Point Approach to Gas Turbine On-Design Cycle Analysis for Aircraft Engines*. Thesis, Daniel Guggenheim School of Aerospace Engineering, 2009.

[39] L. A. McCullers. Aircraft configuration optimization including optimized flight profiles. Conference Paper 87N11743, NASA, January 1984.

[40] Dawn C. Jegley and Jason A. Corman. Technology maturation report for damage arresting composites under the environmentally responsible aviation project. Technical Memorandum NASA/TM–20220015363, NASA, October 2022.